

Summary

The new design was necessary to minimize the effects of SRRS on the uniformity of the beam. This was accomplished primarily by reconfiguration of the beam-transport mirrors and the addition of the blue relays, which facilitated the mounting of the energy and alignment diagnostics. The relocation of the oscillators and driver lines has made for a more compact configuration that is less costly and easier to operate and align. The refinements to the harmonic-energy diagnostics, power conditioning, and control-system designs are cost-effective solutions to some of the problems inherent to the original design. Completion of these new designs has provided a basis upon which better cost estimates and scheduling can be made. Our efforts will now concentrate on refining these designs and ultimately subjecting them to a final design review, expected to take place about one year after Upgrade Project funds are released to LLE.

ACKNOWLEDGMENT

This work was supported by the U.S. Department of Energy Division of Inertial Fusion under agreement No. DE-FC03-85DP40200.

REFERENCES

1. OMEGA Upgrade Preliminary Design Document, DOE/DP40200-101, Sec 2.3 (1989).
2. LLE Review **44**, 188 (1990).
3. M. Skeldon and R. Bahr, to be published in *Optics Letters*.
4. LLE Review **18**, 56 (1984).
5. LLE Review **44**, 219 (1990).

1.B Stimulated Rotational Raman Scattering in Air

Laser-fusion drivers, such as the OMEGA laser, require the propagation of many high-power laser beams over long paths in air to a target chamber. The threshold for certain nonlinear optical processes such as stimulated rotational Raman scattering (SRRS) in air¹⁻⁴ depends on the product of the laser intensity times the air-interaction length. Due to the high laser intensity-length products envisioned for the ultraviolet beams of the OMEGA Upgrade, the possibility of generating forward SRRS in air is of utmost concern. Moreover, schemes such as smoothing by spectral dispersion (SSD)⁵ used to smooth the intensity distribution on target require the use of large optical bandwidths. The effects of certain bandwidths on the stimulated scattering process have been discussed by others; however, the effects of SSD on the SRRS process have only recently been investigated.⁶ Preliminary experiments have been performed on OMEGA to determine the threshold intensity-length product for the generation of SRRS with various types of bandwidth, including SSD.

Theory

The scattering of light has been studied extensively over the last 100 years. Spontaneous light scattering occurs when optical radiation travels through a medium and is scattered by fluctuations in the refractive index brought about by random local material excitations within the medium. With the invention of the laser, a new type of scattering phenomena known as stimulated scattering was discovered. In stimulated scattering the spontaneously scattered radiation field can be strong enough to beat with the incident field and coherently drive the material excitation. Stimulated scattering occurs in high-intensity light beams of small divergence, and the spectrum of scattered light is significantly narrowed.

SRRS in air is a nonlinear process where the material excitation involves transitions between the molecular rotational levels of the molecules in the air. Since air is 80% nitrogen, the problem is approximated by scattering from N_2 molecules. The process can be modeled by including a nonlinear polarization term P^{NL} in the optical wave equation to account for the response of the medium to the optical fields present in the medium.⁷ The optical wave equation for the total electric field E (i.e., the sum of the laser and scattered fields) in the medium is given by

$$\nabla^2 E(r,t) - \frac{n^2}{c^2} \frac{\partial^2}{\partial t^2} E(r,t) = \frac{4\pi}{c^2} \frac{\partial^2}{\partial t^2} P^{NL}(r,t), \quad (1)$$

where c is the speed of light in vacuum, and n is the refractive index, assumed here to be independent of frequency.

To determine the material equation that describes the response of the medium to the optical fields, we write the energy U of the interaction between the polarizability α of an N_2 molecule and the local electric field E as

$$U = -\frac{1}{2} \sum_{ij} \alpha_{ij} E_i E_j. \quad (2)$$

The force F (torque) driving the rotational oscillation is then given by

$$F = -\sum_k \frac{\partial U}{\partial Q_k} = \frac{1}{2} \sum_{ijk} \left(\frac{\partial \alpha_{ij}}{\partial Q_k} \right) E_i E_j, \quad (3)$$

where Q is the rotational coordinate of the molecule. The collection of these localized rotational oscillations gives rise to a propagating optical phonon wave in the medium. We assume that the rotational oscillations are harmonic, giving the equation of motion for the rotational coordinate Q as

$$\mu \frac{\partial^2 Q_k}{\partial t^2} + \mu \Gamma \frac{\partial Q_k}{\partial t} + \mu \omega_R^2 Q_k = \frac{1}{2} \sum_{ij} \left(\frac{\partial \alpha_{ij}}{\partial Q_k} \right) E_i E_j, \quad (4)$$

where ω_R is the resonance frequency of the rotational oscillation, μ is the reduced mass of the system, and the right-hand side of this equation is the force (torque) driving the rotational oscillations. In this equation, a damping term (second term on the left) has been added phenomenologically where Γ is the damping constant or linewidth for the Raman process. The nonlinear polarization in Eq. (1) can be obtained by expanding the electronic polarizability α of the medium in a Taylor series in one of its rotational coordinates and writing the i^{th} component of the polarization P_i of the medium in the form

$$P_i = \sum_j N(\alpha_{ij})_0 E_j + \sum_{jk} N\left(\frac{\partial\alpha_{ij}}{\partial Q_k}\right) Q_k E_j + \dots, \quad (5)$$

where N is the number of molecules taking part in the interaction. The nonlinear polarization of the medium in Eq. (1) can be approximated by the second term on the right in the above equation. (The first term is the linear term giving rise to the ordinary index of refraction of the medium.) The equation of motion for the optical phonon wave [Eq. (4)] along with the optical wave equation [Eq. (1)], form a set of coupled nonlinear differential equations for the optical fields and molecular rotations. When appropriate boundary conditions are applied, these equations describe the stimulated rotational Raman process in detail.

To solve the above equations we assume that the laser and Stokes fields (for simplicity, we assume only one Stokes field is present) can be represented by plane-wave expansions with slowly varying amplitudes [i.e., $E_i = 1/2 A_i \exp(ik_i z - i\omega_i t) + cc$, with $i = L$ for the laser field and $i = S$ for the Stokes field] and similarly for the material wave [i.e., $Q = 1/2 \tilde{Q} \exp(ik_R z - i\omega_R t) + cc$]. If we substitute these into the above equations and keep only those terms that are properly phase matched, we obtain the set of coupled wave-amplitude equations

$$\frac{\partial}{\partial z} A_L(z,t) + \frac{1}{v_L} \frac{\partial}{\partial t} A_L(z,t) = \frac{i\pi N \omega_L}{nc} \left(\frac{\partial \alpha}{\partial \tilde{Q}} \right) \tilde{Q}(z,t) A_S(z,t) \quad (6a)$$

$$\frac{\partial}{\partial z} A_S(z,t) + \frac{1}{v_S} \frac{\partial}{\partial t} A_S(z,t) = \frac{i\pi N \omega_S}{nc} \left(\frac{\partial \alpha}{\partial \tilde{Q}} \right) \tilde{Q}^*(z,t) A_L(z,t) \quad (6b)$$

$$\frac{\partial}{\partial t} \tilde{Q}(z,t) + \frac{\Gamma}{2} \tilde{Q}(z,t) = \frac{i}{4\mu\omega_R} \left(\frac{\partial \alpha}{\partial \tilde{Q}} \right) A_L(z,t) A_S^*(z,t). \quad (6c)$$

In deriving these equations we have assumed conservation of energy ($\omega_L - \omega_S = \omega_R$) and the phase-matching condition $k_L - k_S = k_R$. It can be seen from Eq. (6c) that the material response \tilde{Q} is driven by the beating of the laser and Stokes fields.

The above coupled wave-amplitude equations can be solved if we assume that the laser field is nondepleted. The steady-state solution (neglecting time derivatives) for the Stokes intensity can be calculated by neglecting the first equation above and assuming the laser field to be constant in the second and third equations. The result gives

$$I_S(L) = I_S(0)\exp(gI_L L), \quad (7)$$

where we have used the definition of the intensity for wave i

$$I_i = ncA_i A_i^* / 8\pi,$$

$I_S(0)$ is the noise field to be amplified by the nonlinear process, L is the interaction length, and

$$g = \frac{8\pi^2 N \omega_S}{n^2 c^2 \mu \omega_R \Gamma} \left(\frac{\partial \alpha}{\partial \tilde{Q}} \right)^2 \quad (8)$$

is the steady-state gain coefficient for rotational Raman scattering. The gain coefficient can also be expressed in terms of a spontaneous scattering cross section; however, this gain coefficient can be measured and is known and tabulated for many materials.⁷ From Eq. (7), it can be seen that Raman scattering is similar to a pure gain process with an exponential gain coefficient proportional to the pump-laser-intensity-length product. If the pulse width of the pump laser is of the order of the response time of the medium then a steady-state solution is not valid and a transient solution must be used. The above equations can be solved (again assuming a nondepleted pump) to give the transient solution⁷

$$I_S(L, t) = I_S(0, t) \exp \left[2(gI_L L t / \tau_R)^{1/2} - t / \tau_R \right] \quad (9)$$

for the intensity of the Stokes field in the medium where $\tau_R = 1/\Gamma$ is the response time for SRRS.

In Eqs. (7) and (9), the most difficult input parameter to model is the noise intensity $I_S(0, t)$ that seeds the interaction at $z = 0$ and grows into the output Stokes signal. This noise intensity is due to spontaneous Raman scattering of pump-laser photons into the Stokes wave. Only those noise photons scattered into a small frequency interval and small solid angle in the forward direction will experience appreciable gain throughout the interaction length. For typical experimental conditions, the pump-laser intensity (I_L^{th}) needed to reach SRRS threshold can be obtained by setting the argument of the exponential in Eq. (9) equal to 30 giving

$$I_L^{th} = \frac{(30 + t / \tau_R)^2}{4gLt / \tau_R}. \quad (10)$$

This definition of threshold can be interpreted as the pump-laser intensity required for the Stokes intensity to grow to 1% of the pump-laser intensity (i.e., $I_S = 0.01 I_L^{th}$). From this analysis, the noise intensity $I_S(0, t)$ in Eq. (9) that seeds the SRRS process can be approximated as

$$I_S(0, t) = \frac{0.01}{4gLt / \tau_R} (30 + t / \tau_R)^2 \exp(-30). \quad (11)$$

For short pulses, Eq. (9) with Eq. (11) can be used to approximate the Stokes signal generated by an intense laser beam propagating over a long air path.

The above discussion assumed that the optical fields could be represented as plane waves with slowly varying amplitudes. The analysis should also hold for an input field with a bandwidth $\Delta\omega$ due to phase modulation. For the case of a large phase-modulated bandwidth $\Delta\omega \gg \tau_R^{-1}$, one should not use $t = \Delta\omega^{-1}$ as the time in the transient gain formula Eq. (9); although the phase of the pump laser is changing with time, the noise field that seeds the Raman process and experiences the highest gain throughout the process will be that which has a phase modulation replicating the phase modulation of the pump laser. Hence, the result is that the threshold for SRRS is independent of bandwidth for a phase-modulated input pump beam.

The above analysis assumed only a single Stokes field was present. In a diatomic gas such as the nitrogen molecules in air, the quantum-selection rules allow the rotational quantum number J to change by 0 and ± 2 . For $\Delta J = 0$ the gain for SRRS is 0, and for $\Delta J = -2$ the gain is negative. Hence, for positive SRRS gain, only the $\Delta J = +2$ transitions (S transitions) will contribute. The spectrum of SRRS will then consist of discrete lines spaced by

$$\Delta\nu = 4B \left(J + \frac{3}{2} \right) \quad (12)$$

from the pump laser, where B is the rotational constant equal to 2 cm^{-1} for nitrogen.¹

Experimental Results

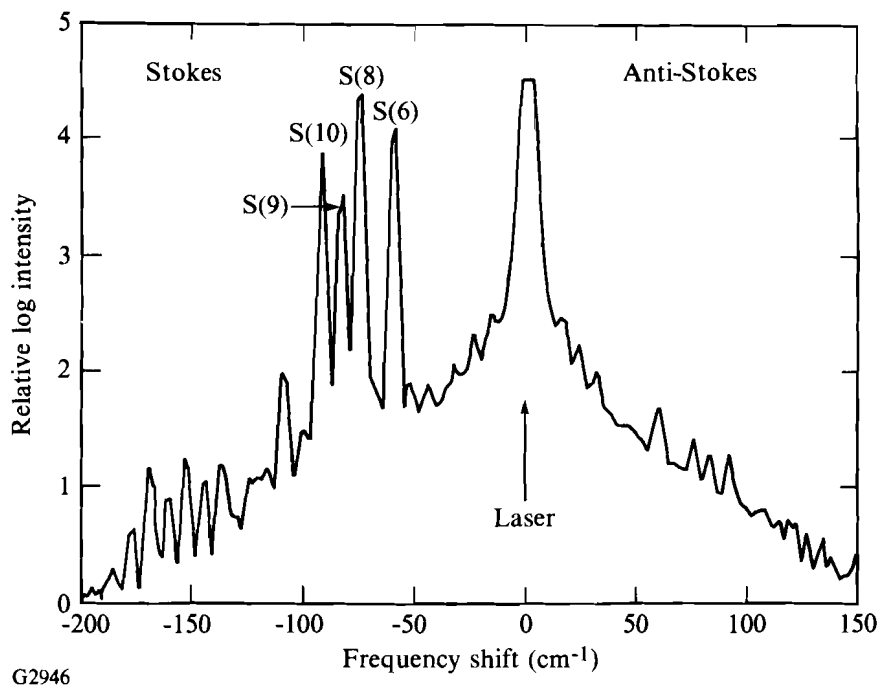
To determine the effects of pure phase-modulated bandwidth on the SRRS process, the gratings in the OMEGA driver line were removed, and the LiNbO₃ electro-optic modulator was used to impose a sinusoidal phase modulation with 8.45-GHz modulation frequency onto the beam. This phase-modulated pulse was then amplified by one beamline of the OMEGA laser. The frequency-tripled output from this beamline was down-collimated to a 5-cm beam diameter and propagated over a distance of 35 m in air. At the end of the path the beam was analyzed with a 1-m Spex spectrometer having a 1200-lines/mm grating used in second order. The energy of the beam was varied up to 20 J per pulse and measured with calibrated detectors.

The spectroscopic data was recorded with Kodak Aerographic Duplicating Film 4421 with a peak spectral sensitivity near 350 nm. To calibrate the film, a wedged etalon provided calibrated laser pulses varying in energy. The etalon was coated for 70% reflection on each side, yielding a factor-of-2 change in intensity between successive pulses transmitted through the tilted etalon and sent to the film. The film was then digitized with a microdensitometer and a density-log-intensity (D-log-I) curve was constructed giving a usable peak film density of ~ 4 . This enabled detection of the faint Stokes and anti-Stokes lines while not saturating the fundamental laser line.

A typical Raman spectrum is shown in Fig. 44.8, where the laser line at $\Delta\nu = 0$ was intentionally saturated to better illustrate the SRRS spectrum. In this spectrum, the four strong Raman lines on the Stokes side of the laser can be identified as the S(6), S(8), S(9), and S(10) lines from nitrogen. The corresponding second Stokes and anti-Stokes lines of these transitions can also be seen. In addition to these four lines, several other lines can be identified corresponding to other rotational levels as well as lines due to the scattering off more than one rotational level. Note that odd J -value transitions, such as the S(9) and others not previously reported, are clearly seen in the Stokes and anti-Stokes spectra. The overall envelope to this spectrum is due to scattering of the highly saturated laser radiation in the film emulsion. This envelope disappears when the film is not saturated with laser light.

Fig. 44.8

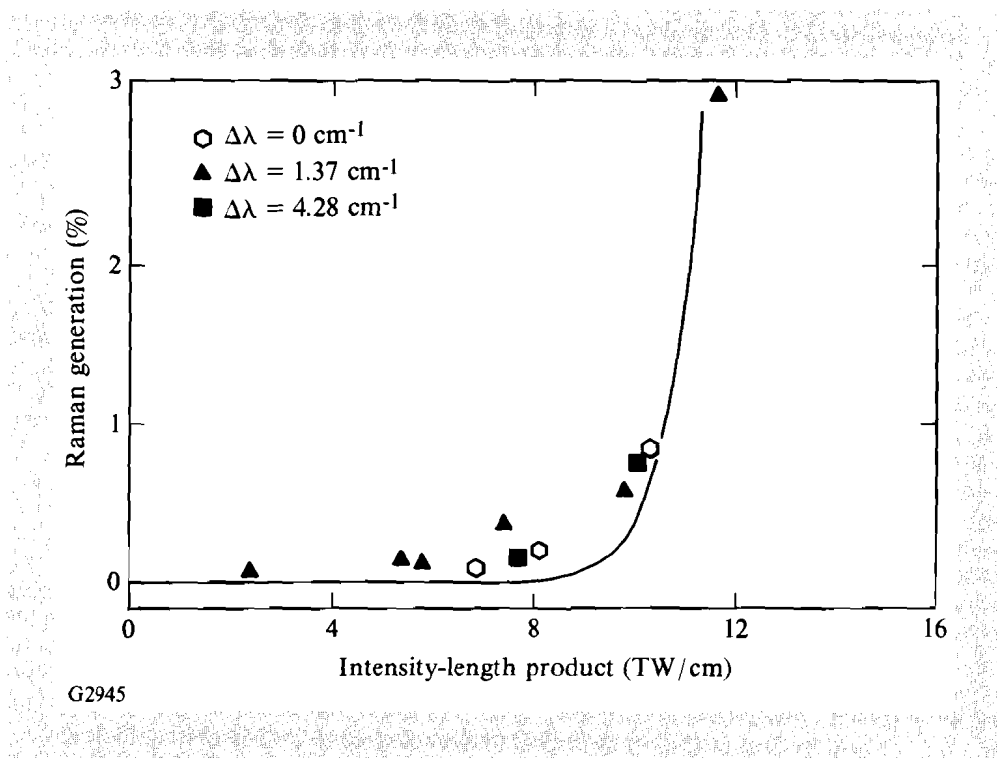
Raman spectrum showing several of the S transitions of nitrogen in air. The pump laser saturated the film at $\Delta\nu = 0$.



To measure the threshold for SRRS, spectra from several laser pulses were processed to obtain the Raman Stokes energy for each laser pulse. The film was first linearized in intensity using the D-log-I calibration curves described above. The energy on the film was then integrated along the spectrometer exit-slit direction to produce a calibrated intensity profile of the Raman spectra similar to the saturated profile of Fig. 44.8. The area under the laser line on the spectra was then compared to the area under all the Stokes lines giving the ratio of laser energy scattered into all the Stokes lines. The measured laser energy was then used to calculate the energy scattered into all of the Stokes lines.

In Fig. 44.9, the percent of Stokes energy generated is plotted versus the pump-laser-intensity-length product. The near-field intensity profiles of the laser pulses were also recorded on film and indicate that the beam had many intensity "hot spots" within the beam aperture. The laser-intensity-length product plotted in Fig. 44.9 is the laser energy measured with the calibrated detectors, multiplied by the interaction length, divided by the pulse width and beam area, and multiplied by a parameter to account for the intensity hot spots in the beam. In Fig. 44.9, the percent of Raman Stokes energy generated is the ratio of the area under the Stokes lines in the spectra to that of the pump. Figure 44.9 shows the SRRS threshold for three different bandwidths at 351 nm: no phase-modulated bandwidth ($\Delta \lambda = 0 \text{ cm}^{-1}$), 1.37 cm^{-1} , and 4.28 cm^{-1} . The solid curve in Fig. 44.9 is the theoretical calculation of the percent of Stokes energy generated [from Eqs. (9) and (11) assuming the same Stokes pulse width and beam area as the pump laser] plotted versus the pump-laser-intensity-length product.

Fig. 44.9
Threshold for SRRS in air with 0 cm^{-1} , 1.37 cm^{-1} , and 4.28 cm^{-1} of phase-modulated bandwidth.

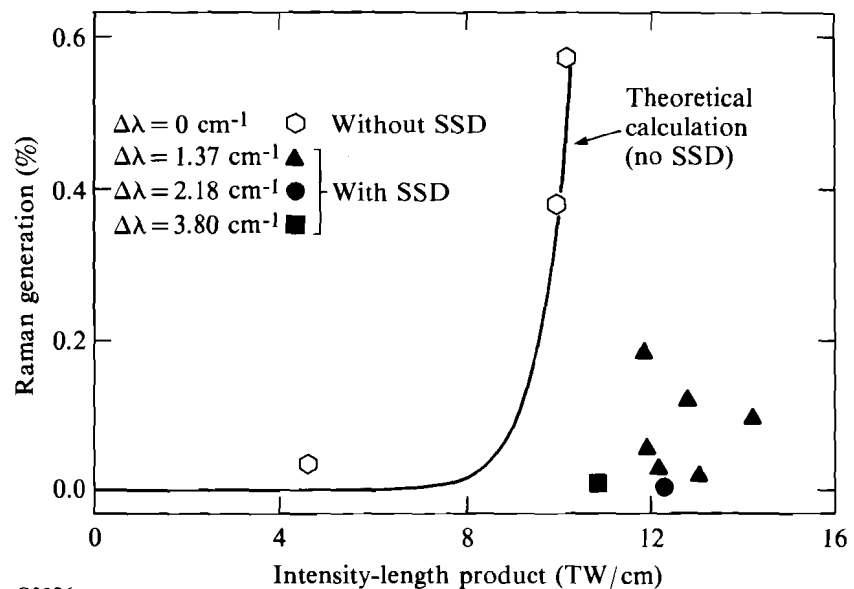


The wavelength dependence of the gain coefficient g has been calculated³ and for 351 nm in air is ~ 7.5 cm/TW (see for example, Fig. 2 of Ref. 3). The remaining parameters used in this calculation that give the best fit to the data are $I_S(0, t)$ from Eq. (11), the laser pulse width $t = 500$ ps, the response time for SRRS $\tau_R = 133$ ps,^{2,8} and the interaction length $L = 35$ m. A hot-spot parameter of 2 was used for all of the data points. From Fig. 44.9 we note that the threshold for SRRS in air is unaffected by the introduction of up to 4.28 cm⁻¹ of phase-modulated bandwidth.

To test the effect of SSD on the SRRS process, SSD was installed on the OMEGA laser and the above experiment was repeated. The angular spectral dispersion of the beam used in the experiment was 74 μ rad/cm⁻¹ at 351 nm in one dimension at the output of the down collimator. The virtual image of the second grating (after taking into consideration the image relaying throughout the OMEGA beamline and the down collimator) was located at a distance of ~ 2.5 m before the beginning of the 35-m, down-collimated beam path. For example, with an applied SSD bandwidth of 3.80 cm⁻¹ the divergence of the beam is 282 μ rad in one direction, due to angular spectral dispersion, and diffraction limited in the orthogonal direction. This bandwidth increases the beam area at the end of the path by $\sim 28\%$ and provides "smoothing" of the beam-intensity profile.⁵ All other parameters of the experiment were identical to the pure phase-modulated bandwidth above.

Fig. 44.10
Threshold for SRRS in air with 0 cm⁻¹, 1.37 cm⁻¹, 2.18 cm⁻¹, and 3.80 cm⁻¹ of phase-modulated bandwidth with SSD.

Figure 44.10 shows the threshold for SRRS with and without SSD. In this figure four different bandwidths are shown: no SSD bandwidth ($\Delta\lambda = 0$ cm⁻¹), 1.37 cm⁻¹, 2.18 cm⁻¹, and 3.80 cm⁻¹. To obtain the laser-



G2926

intensity-length product for the data in this figure, the laser intensity was integrated over the beam path, i.e.,

$$\int_0^L I_L(z) dz,$$

to account for the applied angular spectral dispersion. For best fit to the data, the same parameters as above were used in the no-bandwidth theoretical calculation (solid curve) and a hot-spot parameter of 3 was used for all of the data points. (Due to the increased divergence of the laser with SSD, larger pinholes were used in the spatial filters resulting in an increase in the intensity modulation of the beam.) It can be seen from Fig. 44.10 that the threshold for SRRS increased for 1.37 cm^{-1} of SSD bandwidth. In addition, for 2.18 cm^{-1} and 3.80 cm^{-1} of SSD bandwidth, no SRRS signal was recorded when the pump laser intensity-length product was above the no-bandwidth threshold for SRRS.

We conclude from the excellent theoretical fit to the data that the simple models for SRRS hold for our experimental conditions. In particular, SRRS generated by the frequency-tripled output from a large Nd:glass laser is seeded by the usual noise mechanisms; a transient solution for laser pulses of 500-ps pulse width is appropriate; and the SRRS gain coefficient is $\sim 7.5 \text{ cm/TW}$ at 351 nm. The threshold for SRRS is unaffected by the application of up to 4.28 cm^{-1} of pure phase-modulated bandwidth with 8.45-GHz modulation frequency. The threshold for SRRS, on the other hand, increases with as little as 1.37 cm^{-1} of SSD bandwidth.

ACKNOWLEDGMENT

This work was supported by the U.S. Department of Energy Division of Inertial Fusion under agreement No. DE-FC03-85DP40200 and by the Laser Fusion Feasibility Project at the Laboratory for Laser Energetics, which has the following sponsors: Empire State Electric Energy Research Corporation, New York State Energy Research and Development Authority, Ontario Hydro, and the University of Rochester.

REFERENCES

1. V. S. Averbakh, A. I. Makarov, and V. I. Talanov, *Sov. J. Quantum Electron.* **8**, 472 (1978).
2. M. A. Henesian, C. D. Swift, and J. R. Murray, *Opt. Lett.* **10**, 565 (1985).
3. M. Rokni and A. Flusberg, *IEEE J. Quantum Electron.* **QE-22**, 1102 (1986).
4. A. Ori, B. Nathanson, and M. Rokni, *J. Phys. D: Appl. Phys.* **23**, 142 (1990).
5. S. Skupsky, R. W. Short, T. Kessler, R. S. Craxton, S. Letzring, and J. M. Soures, *J. Appl. Phys.* **66**, 3456 (1989). See also LLE Review **37**, 29 (1988).